UC Davis

Title

Inhibition of EphB4-Ephrin-B2 Signaling Reprograms the Tumor Immune Microenvironment in Head and Neck Cancers.

Permalink

https://escholarship.org/uc/item/7ck792jw

Journal

Cancer Research, 79(10)

Authors

Bhatia, Shilpa

Oweida, Ayman

Lennon, Shelby

et al.

Publication Date

2019-05-15

DOI

10.1158/0008-5472.CAN-18-3257

Peer reviewed

Inhibition of EphB4-ephrin-B2 signaling reprograms the tumor immune microenvironment in head and neck cancers

Shilpa Bhatia[1], **Ayman Oweida**[1], **Shelby Lennon**[1], **Laurel B. Darragh**[1], **Dallin Milner**[1], **Andy V. Phan**[1], **Adam C. Mueller**[1], **Benjamin Van Court**[1], **David Raben**[1], **Natalie J. Serkova**[2], **Xiao-Jing Wang**[3,4], **Antonio Jimeno**[5], **Eric T. Clambey**[2], **Elena B. Pasquale**[6], and **Sana D. Karam**[1,*]

[1]Department of Radiation Oncology, University of Colorado Denver, Anschutz Medical Campus, Aurora, CO 80045, USA

[2]Department of Anesthesiology, University of Colorado Denver, Anschutz Medical Campus, Aurora, CO 80045, USA

[3]Department of Pathology, University of Colorado Denver, Anschutz Medical Campus, Aurora, CO 80045, USA

[4]Veterans Affairs Medical Center, VA Eastern Colorado Health Care System, Aurora, CO 80045, USA

[5]Division of Medical Oncology, Department of Medicine, University of Colorado Denver, Anschutz Medical Campus, Aurora, CO 80045, USA

[6]Cancer Center, Sanford Burnham Prebys Medical Discovery Institute, La Jolla, CA 92037, USA

Abstract

Identifying targets present in the tumor microenvironment that contribute to immune evasion has become an important area of research. In the current study, we identified EphB4-ephrin-B2 signaling as a regulator of both innate and adaptive components of the immune system. EphB4 belongs to receptor tyrosine kinase family that interacts with ephrin-B2 ligand at sites of cell-cell contact resulting in bidirectional signaling. We found that EphB4-ephrin-B2 inhibition alone or in combination with radiation (RT) reduced intratumoral regulatory T cells (Tregs), and increased activation of both CD8+ and CD4+Foxp3- T cells compared to the control group in an orthotopic head and neck squamous cell carcinoma (HNSCC) model. We also compared the effect of EphB4-ephrin-B2 inhibition combined with RT to combined anti-PDL1 and RT and observed similar tumor growth suppression, particularly at early time-points. A patient-derived xenograft model showed reduction of tumor-associated M2 macrophages and favored polarization towards an anti-tumoral M1 phenotype following EphB4-ephrin-B2 inhibition with RT. *In vitro*, EphB4 signaling inhibition decreased Ki67-expressing Tregs and Treg activation compared to the control group. Overall, our study is the first to implicate the role of EphB4-ephrin-B2 in tumor immune response. Moreover, our findings suggest that EphB4-ephrin-B2 inhibition combined with RT represents a

---

potential alternative for HNSCC patients and could be particularly beneficial for patients who are ineligible to receive or cannot tolerate anti-PDL1 therapy.

Keywords

Head and Neck cancer; EphB4; Ephrin-B2; Immune remodeling; Tumor microenvironment

Introduction

Numerous clinical trials are testing the benefits of immunotherapy in human cancer, including head and neck squamous cell carcinoma (HNSCC). The objective response rate is 6–20% (1–4) and the vast majority of patients demonstrate either innate or adaptive resistance to immunotherapy. Clinical trial study attempts at simply combining more immune checkpoint inhibitors have also proven disappointing due to increased toxicity to patients and lack of additional benefit (NCT02205333). In orthotopic mouse models of HNSCC, we have recently demonstrated that tumor regrowth occurs even after combination treatment with anti-PDL1 antibody and radiation therapy (RT) (5).

Concerted efforts to understand the factors involved in resistance to immunotherapy within the tumor microenvironment (TME) have led to the identification of T regulatory cells (Tregs) and tumor-associated macrophages (TAMs) as key regulators of tumor growth and therapeutic response. Our laboratory recently showed an increase in the Treg population during tumor regrowth phase of anti-PDL1 antibody treatment combined with RT in preclinical HNSCC mouse models (5). Studies have shown a correlation between high Treg/TAM infiltrates and poor survival outcomes (6,7). Targeted depletion of Tregs or TAMs has been reported to improve the response to chemotherapy and checkpoint inhibitors in different tumor models (8,9). However, data from clinical trials suggest lack of efficacy following treatment with Treg-targeted immunotherapies such as anti-CTLA-4 (10). Therefore, there is an unmet need for alternate approaches that can both target immunosuppressive cell populations within the TME and enhance therapeutic benefit.

EphB4 belongs to the largest family of receptor tyrosine kinases and upon interaction with the ephrin-B2 ligand has been reported to regulate neuronal migration, bone remodeling, angiogenesis, cancer progression, and metastasis (11). EphB4 and ephrin-B2 expression is downregulated in vast majority of adult normal tissues, even as early as postnatal development but its overexpression has been implicated during malignant transformation (12–14). Thus, targeting of EphB4-ephrin-B2 represent a therapeutic strategy that has survived the test of clinical trials. It has been shown to be safe in multiple clinical trials (NCT01642342, NCT02717156, NCT02767921) with minimal to no toxicity (15), likely due to low levels of expression in normal tissue. In our laboratory, we have previously shown that EphB4-ephrin-B2 inhibition in different patient-derived xenograft (PDX) HNSCC models enhances tumor response to RT (16) as well as to combined EGFR inhibition and RT (17). While direct evidence that implicates EphB4-ephrin-B2 interaction in the cancer-related immune response is lacking, multiple reports have documented that Eph/ephrin gene family members modulate immune cell processes in inflammatory models,

such as arteriosclerosis and wound healing (18–20). Eph-ephrin interactions have also been reported to regulate monocyte adhesion to the blood vessel wall (18), trans-endothelial migration (20,21), T cell activation, proliferation and apoptosis (22,23), and mobilization of hematopoietic cells from bone marrow sinusoids (24).

In the current study, we sought to determine whether inhibition of EphB4-ephrin-B2 interaction can induce an anti-tumor immune response in HNSCC. Our data show that EphB4 is expressed in HNSCC tumor and stromal cells. Based on these findings, and the role of Eph/ephrins in immune processes in inflammatory models, we hypothesized that EphB4-ephrin-B2 interaction regulates the tumor immune microenvironment by sustaining Tregs and TAMs, thus negatively impacting the ability of CD8+ T cells to induce an anti-tumor response. We demonstrate that targeted blockade of EphB4-ephrin-B2 signaling results in a significant tumor growth retardation and remodeling of the immune landscape in a HNSCC orthotopic immunocompetent model and in a PDX model. We also compared the relative efficacy of EphB4-ephrin-B2 inhibition combined with RT (which is a mainstay for the treatment of HNSCC) to the anti-PDL1 therapy and RT combination. We observed a similar tumor growth inhibition response with both treatments at early time-point. In conclusion, our study is the first report providing insight into a novel role of EphB4-ephrin-B2 interaction in modulating the tumor immune microenvironment in HNSCC.

Methods

Cell culture and reagents

The murine Moc2 cell line was obtained from Dr. Ravindra Uppaluri (Dana-Farber Cancer Institute, MA) and the Ly2 cell line was obtained from Dr. Nadarajah Vigneswaran (University of Texas Health Science Center, TX). Ly2 cells were cultured in DMEM-F12 and Moc2 cells in IMDM medium. The medium was supplemented with 10% FBS and 1% primocin and cells were cultured at 37°C in a 5% CO_2 incubator. All the cell lines used in this study were within 12 passages and were tested for mycoplasma contamination. The short tandem repeat (STR) analysis was performed as a method of authentication wherever applicable. The soluble EphB4 extracellular domain fused to human serum albumin (sEphB4-HSA) (16) was used to inhibit EphB4-ephrin-B2 interaction in a PDX immunocompromised mouse model. The sEphB4-HSA protein was provided by Vasgene Therapeutics, Inc. (Los Angeles, CA, USA). For immunocompetent mouse models, a plasmid encoding the 15 amino acids long TNYL-RAW peptide fused with the Fc portion of human IgG1 (TNYL-RAW-Fc, an EphB4 antagonist) was used to block EphB4-ephrin-B2 signaling (25). pcDNA3 plasmid was used as a control. The plasmids were obtained from Dr. Elena Pasquale's lab (Sanford Burnham Prebys Medical Discovery Institute, CA). The PEGylated form of TNYL-RAW peptide was obtained from Anaspec (Fremont, CA) for *in vitro* studies involving T cells (26).

HNSCC Patient samples

Excess, non-diagnostic fresh tumor tissue was collected from HNSCC patients with informed consent at the University of Colorado Hospital in accordance with the protocol approved by the Colorado Multiple Institutional Review Board (COMIRB # 08–0552).

Following tumor resection, tumor tissues were analyzed by a clinical pathologist and non-necrotic sections were used for research purposes including establishment of patient-derived xenograft model.

In vivo models

All mice were handled and euthanized in accordance with the ethics guidelines and conditions set and overseen by the University of Colorado, Anschutz Medical Campus Animal Care and Use Committee. The study has been approved by the Institutional Animal Care and Use Committee (IACUC). For immunocompromised mouse model studies, female athymic nude mice (5–6 weeks old, n=5–7 per group) were used. The HNSCC PDX tumors CUHN013 and CUHN004 (F8–F16 generation) were obtained from Dr. Antonio Jimeno's lab (University of Colorado, Anschutz Medical Campus, Aurora, CO). Tumor implantations were performed as described earlier (16). When tumor volumes reached approximately 50–150 mm^3, mice were randomized into four groups (1) PBS, (2) sEphB4-HSA, (3) PBS+RT, and (4) sEphB4-HSA+RT. Mice were either injected with PBS or with a 20 mg/kg dose of sEphB4-HSA (three times/week) and/or subjected to RT (5 Gy/fraction × 4 fractions) as described earlier (16).

For iron oxide imaging studies, superparamagnetic iron oxide (SPIO) nanoparticles were generated (27). The detailed protocol for magnetic resonance (MR) imaging as reported by Serkova et al. (27) was followed. MR imaging was performed before treatment and 96 hours after the last dose of RT. Final images were processed with ParaVi-sion software (Bruker Biospin).

For immunocompetent mouse model studies, 5–6 week old female BALB/c mice (n=7–8) (Charles River Laboratories, Wilmington, MA) or C57BL/6 mice (n=7–8) (Jackson Laboratories, Bar Harbor, ME) were used. Tumor cell inoculation was performed as described earlier (28). Mice were randomized at day 4–5 post-tumor inoculation (tumor volume ~ 50 mm^3) to receive either pcDNA3 control plasmid or TNYL-RAW-Fc plasmid (20 μg in ~2 ml of PBS) via hydrodynamic injection (24) and tumor size was measured biweekly as described earlier (28). For combination therapy studies, mice were randomized into IgG+pcDNA3 control, IgG+TNYL-RAW-Fc, anti-PDL1+TNYL-RAW-Fc, RT+IgG +pcDNA3, RT+IgG+TNYL-RAW-Fc, RT+anti-PDL1+pcDNA3, and RT+anti-PDL1+TNYL-RAW-Fc. IgG2b control (referred as IgG; BioXcell, NH) and anti-PDL1 (BioXcell, NH) were administered on day 7–9 after tumor inoculation by intraperitoneal method at a dose of 10 mg/kg twice a week throughout the course of experiment. RT was administered at a single dose of 10 Gy as described earlier (28). Plasmid DNA treatment was initiated on day 5 after tumor inoculation and administered as a single dose. Tumor tissue was harvested at the time of sacrifice and either fixed in 10% neutral buffered formalin or flash-frozen for further analysis.

Immune cell depletion studies

CD8 T cell depletion was performed using an anti-CD8 antibody (Clone 53–6.7, 10 mg/kg, i.p. BioXcell, NH) and the corresponding rat IgG1 isotype was used as a control. The antibodies were administered 1 week prior to tumor implantation and were continued once a

week for 3 weeks after tumor implantation. TNYL-RAW-Fc or pcDNA3 treatment was performed on day 4 after tumor implantation because of the aggressive nature of tumor models used in this study. Flow cytometry was performed to confirm systemic depletion of CD8+ T cells by using an anti-CD8 antibody clone that do not compete with clone 53–6.7 used for depletion experiment.

Flow cytometry

Tumors and spleens were processed into single-cell suspensions for flow cytometric analysis as described earlier (28) and 1–2×10^6 live cells were plated in a 96-well plate followed by blocking with anti-CD16/32 antibody. For analysis of immune cells, cytokines, and phospho-STAT3 marker, the following conjugated antibodies were used: AlexaFluor700-CD45 (1:50, Clone 30-F11, cat#56-0451-82, eBioscience), BUV737-CD11b (1:100, Clone M1/70, cat#564443, BD Biosciences), FITC-F4/80 (1:100, Clone BM8, cat#123108, Biolegend), DyLight350-CD3 (1:100, Clone 145–2C11, Novus Biologicals), eFluor450-CD4 (1:100, Clone RM4–5, cat#48-–0042-82, eBioscience), APC-eFluor780-CD8 (1:100, Clone 53–6.7, cat# 47-0081-82, eBioscience), PECyanine7-IFNγ (1:20, Clone XMG1.2, cat#25-7311-82, eBioscience), Ki67-BV605 (1:50, Clone 16A8, cat#652413, eBioscience), p-STAT3-PE (1:5, clone 49; p727, cat#558557, eBioscience).

For cytokine release experiments, single cell suspensions were plated in 6-well plates in the presence of monensin (to block cytokine release) and a cell activation cocktail with Brefeldin to stimulate cytokine production at 37°C for 3.5–4 hours. After washes, the cells were stained with surface marker antibodies (1:100 dilution) at room temperature for 30 min. Cells were then resuspended in 100 μl of Cytofix/Cytoperm™ solution (BD Biosciences) for 20 min at 4°C. Following incubation, cells were washed with 1X Perm/Wash™ solution (BD Biosciences), and stained with anti-cytokine antibodies at 4°C for 30 min. Cell pellets were resuspended in FA3 buffer and samples were run on the YETI cell analyzer. To detect STAT3 phosphorylation (p-STAT3) and Ki67 expression in cultured T cells by flow cytometry, single cell suspensions treated with pre-clustered control Fc, 20 μg/ml ephrin-B2-Fc, or PEGylated TNYL-RAW (4.5 μg/ml) following treatment with stimulating dose of ephrin-B2-Fc (2.5 μg/ml) for 24–48 h were stained with immune cell surface markers. This was followed by incubation in 1X lyse/fix buffer (BD Biosciences) at 37°C for 30 min. Pre-clustering was performed by incubating Fc proteins with hIgG in the ratio of 1:3 at 4°C for 30 min in an orbital shaker. Following washing with PBS, samples were resuspended in cold perm III buffer (BD Biosciences), incubated on ice for 15 min, and stained with p-STAT3 or Ki67 antibodies for 30 min at room temperature. Various controls such as beads only, samples stained with a single antibody, isotype controls, and fluorescence minus-one (FMO) controls were also included. Live cells were gated using Aqua/vi live/dead stain. Stained cells were run on the YETI Cell Analyzer at the University of Colorado Denver Cancer Flow Cytometry Core. Data was analyzed using Kaluza analysis software.

RNA extraction and qPCR analysis

Tregs and monocytes were harvested from Ly2 tumors using isolation kits (Stemcell Technologies). Monocytes were treated with IL-4 (25 ng/ml) to allow differentiation into M2

macrophages (29,30). Total RNA was collected from Tregs and macrophages using RNeasy mini prep kits (Qiagen). cDNA was prepared as described earlier (28). Aliquots (2 μL) of a 1:2 dilution of the reverse transcription reactions were subjected to quantitative real-time PCR with the following primers using a iQ real time-PCR detection system (BioRad). GAPDH mRNA levels were analyzed as a housekeeping gene for normalization purposes. Similar RNA extraction and qPCR protocol was used to detect mRNA levels of EPHB4 and EFNB2 in Ly2 tumors in the absence and presence of 10 Gy dose of RT.

GAPDH: Forward primer: 5'CGTGGAGTCTACTGGCGTCTT3'

Reverse primer: 5'CGGAGATGATGACCCTTTTGG3'

EPHB4: Forward primers: 5'GGATCGCATTCAGCCAAAGT3'

5'GGCACCTGGTTCCACTATCT3'

Reverse primers: 5'ACTGTCTAAGGCTGTGGCAT3'

5'CCATTTCAGATCCGCCGTTT3'

EFNB2: Forward primer: 5'TAAAGACCAAGCAGACAGATGCAC3'

Reverse primer: 5'GTGATGATGATGACGATGAAGATG3'

Mass cytometry (CyTOF)

For mass cytometry experiments, tumors were harvested and digested as described above in the flow cytometry section. Single cell suspensions were washed with PBS and stained with heavy-metal tagged antibodies according to manufacturer instructions (Fluidigm, San Francisco, CA). The following antibodies were used: CD45-Y89 (cat#3089005B), CD3e-Sm152 (cat#3152004B), FoxP3-Gd158 (cat#3158003A), CD4-Nd145 (cat#3145002B), CD8a-Er168 (cat#3168003B), CD11b-Nd148 (cat#3148003B), F4/80-Nd146 (cat#3146008B), CD11c-Nd142 (cat#3142003B), Ly6G-Pr141, Ly6C-Nd150, ICOS-Yb176 (cat#3176014B), and live-dead-Pt-195. Stained cells were run on the Helios Mass Cytometer at the University of Colorado Denver Cancer Center Flow Cytometry Core. Data were analyzed using Kaluza or FlowJo Analysis software.

Immunoblotting

For immunoblotting, protein cell lysates were prepared and ran onto 10% SDS-PAGE gels followed by transfer to PVDF membranes and western blotting. Blots were probed overnight at 4°C with primary antibodies. Anti-p-AKT (1:1000, cat#4058), anti-AKT (1:1000, cat#9272), anti-Bcl-XL (1:1000, cat#2764), anti-cleaved caspase-3 (1:1000, cat#9579) and anti-β-actin antibodies (1:5000, cat#12262) were purchased from Cell Signaling Technology (Danvers, MA, USA). Anti-EphB4 (clone m265) was provided by Vasgene Therapeutics Inc. (Los Angeles, CA, USA) or purchased from R&D Systems (cat#AF446). Horseradish peroxidase (HRP)-conjugated secondary antibodies were obtained from Sigma (St. Louis, MO, USA). For p-EphB4 analysis, CD4+ T cells were isolated from mouse splenocytes using EasySep CD4+ T cell isolation kit (Stemcell Technologies) and seeded in a 6-well

plate followed by treatment with pre-clustered control Fc, ephrin-B2-Fc (20 µg/ml), or PEG-TNYL-RAW-Fc (4.5 µg/ml) with ephrin-B2-Fc (2.5 µg/ml) at 37°C for 72 hours. Pre-clustering was performed as described above. Lysates were collected and run on a 10% SDS-PAGE as described above. Membranes were probed with p-EphB4 (1:1000, cat#PA5–64792, ThermoFisher) and anti-β-actin antibodies.

Immunofluorescence staining

Immunofluorescence (IF) staining was performed on paraffin-embedded sections fixed in 4% buffered formalin. Tumor tissue was deparaffinized, hydrated, and antigen epitope retrieval was performed. Sections were incubated with primary antibodies overnight at 4°C. The following antibodies were used: CD107b (1:100, cat#550292, BD Pharmingen), CD163 (1:100, cat#orb13303, Biorbyt), Gpr18 (1:100, cat#NBP2–24918SS, Novus Biologicals), F4/80 (1:50, cat#NB600–404SS, Novus Biologicals), Foxp3 (1:1000, cat# ab20034, Abcam), F4/80 (1:100, cat# 70076, Cell Signaling), and Pan-Keratin (1:100, cat# 4545, Cell Signaling). Primary antibody incubation was followed by treatment with AlexaFlour-tagged IgG secondary antibody (1:400 dilution, Life Technologies). Nuclei were counterstained with 6-diamidino-2-phenylindole dihydrochloride hydrate (DAPI). Images were captured with a 20x objective using a Nikon fluorescence or Olympus confocal microscope. Analysis was performed on 6–8 random fields for each of the experimental and control groups.

ELISA

Plasma samples collected from TNYL-RAW-Fc and pcDNA3 control mice were isolated and subjected to ELISA to measure the levels of TNYL-RAW-Fc as described earlier (24). To detect TGF-β1 levels, plasma samples or cell culture supernatants/conditioned media were analyzed using a TGF-β ELISA kit (R&D systems) according to the manufacturer's instructions.

U-plex cytokine array

Retro-orbital blood collection was performed on mice 11–18 days after hydrodynamic injection of TNYL-RAW-Fc plasmid (immunocompetent mouse model) or 96 hours after RT (nude mouse model). Plasma was isolated and subjected to U-plex array (Meso Scale Diagnostics, Rockville, MD) according to the manufacturer's instructions.

CIBERSORT, TCGA, and mRNA expression analysis

Gene expression data were obtained from the HNSCC cohort in the TCGA database (n=530). The TCGA provides level 3 RNA-seq data which has been aligned to the reference genome and quantified at the gene transcripts level using RNA-Seq by Expectation Maximization (RSEM) (31). The CIBERSORT analysis was performed as described earlier (32). Macrophage populations were categorized into M1 or M2 subtypes based on markers analyzed in the article published by Newman *et al.* (32). M1 related markers include: ACHE, ADAMDEC1, APOL3, APOL6, APOBEC3A, AQP9, ARRB1, CASP5, CCL19, CCL5, CCL8, CCR7, CD40, CXCL10, CXCL11, CXCL9, TNFAIP6, TNIP3, TRPM4, CD80, IL1B, IL12B, IL2RA and M2 markers include AIF1, ALOX15, ASGR2, CCL13, CCL14, CCL18, CCL23, CD68, CD180, CD209, CD163, CLEC4A, CLEC7A, CLEC10A,

MS4A6A, TLR8, IL21R, EGR2, GSTT1, HRH1, FRMD4A (32). Only cases with a p-value < 0.05, which indicates a reliable estimation of immune cell infiltration, were used for further survival analysis. A cutoff value for M1:M2 of 0.5 was assigned for survival analysis. The correlation analysis between EphB4 or ephrin-B2 and TGF-β, HRH1 was performed on the TCGA HNSCC dataset using R2 analysis platform (https://hgserver1.amc.nl/cgi-bin/r2/main.cgi).

Irradiation

Irradiation was performed either using the RS-2000 irradiator (Rad Source Technologies, GA) at 160kVp, 10 mA or the PXi-225Cx image-guided irradiator (PXi inc, KC) at 225 kVp, 13 mA with 0.3 mm Cu filter. Mice were positioned in the prone orientation and a CT scan was acquired. Treatment planning and radiation dose delivery were performed as described (5). Radiation was delivered at a dose rate of 5.6 Gy/min.

Statistical analysis

Statistical analysis was performed using GraphPad Prism software. All the experiments were performed in duplicate or triplicate and repeated 2–3 times. Statistical analyses of differences between two groups were performed using Student's t-test or one-way ANOVA. The Dunnett's post-hoc test was used for further validation after ANOVA where multiple experimental groups were compared to the control group. A p-value of < 0.05 was considered significant.

Results

In HNSCC tumors, EphB4 is present in cancer cells and highly expressed in both Tregs and macrophages compared to ephrin-B2

To analyze the expression of EphB4 and ephrin-B2, we performed IHC staining using sections of tumors derived from the murine Ly2 HNSCC cell line and of CUHN013 patient-derived xenograft (PDX) tumors. Our data show that EphB4 is expressed in both cancer cells and stroma (Figure 1A). Further confirmation showing EphB4 expression on tumor epithelial cells was done by performing IF staining with anti-EphB4 and pan-keratin antibodies (Supplementary Figure 1) Our data also show ephrin-B2 expression on some cancer cells and stroma (Figure 1A) including α-smooth muscle actin (α-SMA)-expressing fibroblasts (Supplementary Figure 2). We also interrogated the R2 database to analyze the mRNA expression of EphB4 and ephrin-B2 using two different datasets that included different immune cell populations (Figure 1B). The Wicker dataset (GSE28491) and the Salazer dataset (GSE2125) indicated higher expression of EphB4 than ephrin-B2 in both Tregs and macrophages isolated from human samples (Figure 1B). These findings were further confirmed by analysis of the ImmGen database (https://www.immgen.org) (Figure 1C). Our IF data also confirmed expression of EphB4 on both F4/80-expressing macrophages and Foxp3-expressing Tregs whereas ephrin-B2 expression was negligible compared to EphB4 on macrophages in Ly2 tumors (Figure 1D). In addition, we performed qPCR analysis on intratumoral Tregs and macrophages and data show slightly higher levels of EphB4 in intratumoral Tregs compared to ephrin-B2. The EphB4 mRNA levels were

comparatively higher than ephrin-B2 in intratumoral macrophages (Supplementary Figure 3).

Inhibition of EphB4-ephrin-B2 signaling retards tumor growth in mouse orthotopic syngeneic HNSCC models

We previously reported that blockade of EphB4-ephrin-B2 signaling delays tumor growth and enhances radiosensitization in HNSCC PDX models (16). To determine the role of EphB4-ephrin-B2 interaction in supporting tumor growth in immunocompetent models, we used two different orthotopic models of HNSCC: Ly2 (BALB/c) and Moc2 (C57BL/6). The experimental design is presented in Figure 2A. Mice were injected with TNYL-RAW-Fc plasmid, a derivative of the short peptide TNYL-RAW, which very selectively binds to the ephrin-binding pocket of EphB4 and blocks the interaction of the receptor with the ephrin-B2 ligand (26). Although dimerized through the Fc portion, TNYL-RAW-Fc remains an EphB4 antagonist similar to the monomeric peptide. TNYL-RAW-Fc treatment significantly inhibited the growth of both Ly2 (Figure 2B, C) and Moc2 (Figure 2D, E) tumors by 1.53 fold (p=0.03) and 1.61 fold (p=0.02) respectively compared to the pcDNA3 control group. We also determined the circulating levels of TNYL-RAW-Fc by using an Fc-based ELISA assay as described in the methods section. Consistent with the published literature (24), our data show the presence of TNYL-RAW-Fc in the mouse blood 7 days after hydrodynamic injection (p=0.02) (Supplementary Figure 4A).

Inhibition of EphB4-ephrin-B2 interaction significantly decreases Tregs and tumor-associated macrophages and enhances activation of both conventional CD4+Foxp3- and CD8+ T cells in HNSCC tumors

To investigate the contribution of the tumor immune microenvironment to tumor growth retardation due to EphB4-ephrin-B2 inhibition, CyTOF analysis was conducted on Ly2 tumors on days 14 to 18 after administration of the TNYL-RAW-Fc plasmid or pcDNA3 control plasmid. Our data show significant changes in tumor-infiltrating immune cells following TNYL-RAW-Fc treatment (Figure 2F). In particular, CD8+ T cells in the tumors showed a 1.2 fold increase (p=0.03) following TNYL-RAW-Fc treatment compared to pcDNA3 control (Figure 2F). The percentage of CD4+ T cells, however, remained unchanged (Figure 2F). The Treg cells (CD4+ T cells that are also positive for the Foxp3 marker) constitute an important immunosuppressive population in the TME and were dramatically reduced by ~3 fold (p=0.009) in the EphB4-ephrin-B2 inhibited group (Figure 2F). Importantly, the CD8+Teffector cell/Treg ratio that is an indicator of enhanced therapeutic response, also significantly increased (p=0.02) following EphB4-ephrin-B2 inhibition (Figure 2F). Additionally, the activation status of both conventional CD4+Foxp3- T cells and CD8+ T cells, assessed based on ICOS (Inducible T-cell COStimulator) expression (33), showed a ~2.8 fold increase (p=0.0002; p=0.009) following EphB4-ephrin-B2 inhibition (Figure 2F). These activated T cell populations are both known to play a key role in inducing an anti-tumor immune response. The CyTOF data was replicated by flow analysis as shown in Figure 5.

In addition to the changes observed in T cells, we also observed changes in the macrophage population (F4/80+ cells, gated on CD11b+ cells; Figure 2F). There was a 1.9 fold decline

(p=0.04) in the F4/80+ macrophages in the TNYL-RAW-Fc treated group (Figure 2F). Specifically, we noted a 1.4 fold decline (p=0.01) in the pro-tumorigenic M2 macrophages (Arg1+F4/80+ cells) and a 16 fold increase (p<0.0001) in M1 macrophages (F4/80+iNOS+) following TNYL-RAW-Fc treatment (Figure 2F). No significant differences were detected in intratumoral CD11b+Ly6C+ monocytes (Figure 2F) or CD11b+Ly6G+ neutrophils (Figure 2F). We also observed a 1.7 fold upregulation (p=0.01) in the CD11C+ dendritic cell population following EphB4-ephrin-B2 blockade (Figure 2F).

To distinguish whether the observed decrease in Tregs and M2 TAMs in the tumors is a direct effect of intratumoral EphB4-ephrin-B2 inhibition or is due to systemic inhibition (which could decrease exit of these immune cells from the bone marrow, as has been previously reported for hematopoietic stem and progenitor cells (24)), we analyzed blood samples collected from TNYL-RAW-Fc treated and control mice by flow cytometry. Our data demonstrate that in the Ly2 tumor model, TNYL-RAW-Fc treatment does not significantly affect circulating immune cells, including CD45+ cells, CD4+ and CD8+ T cells, Foxp3+ Tregs, CD45+CD11b+ myeloid cells, and F4/80+ macrophages (Supplementary Figure 4B). To confirm the involvement of adaptive immune components, we performed systemic depletion of CD8+ T cells in the BALB/c mouse model, which reversed the effects of TNYL-RAW-Fc enhancing tumor growth (p=0.01) (Supplementary Figure 5A). Depletion of CD8+ T cells was confirmed by flow analysis (p=0.03) (Supplementary Figure 5B).

In vitro inhibition of EphB4 in T cells decreases STAT3 phosphorylation and Ki67 expressing Tregs and alters the levels of key growth-promoting molecules

To understand the mechanisms by which EphB4-ephrin-B2 interaction affects T cell numbers and function in HNSCC tumors, we conducted *in vitro* analyses of CD4+T cells isolated from the spleens of tumor-bearing mice and treated for 72 hours with recombinant ephrin-B2-Fc. We selected recombinant ephrin-B2-Fc protein for *in vitro* studies because at high concentrations (20 μg/ml) it has been reported to inhibit certain EphB4 downstream signals (34). We observed lower levels of tyrosine phosphorylated EphB4 in CD4+ T cells treated with 20 μg/ml ephrin-B2-Fc than in CD4+ T cells treated with Fc control (Figure 3A). To confirm these results, we also treated the CD4+ T cells with PEGylated form of TNYL-RAW peptide EphB4 antagonist (26), also known to block EphB4-ephrin-B2 interaction and observed similar effect.

We examined the effect of ephrin-B2-Fc treatment on Ki67 (a surrogate marker of proliferation) expressing Tregs using flow cytometry and observed that ephrin-B2-Fc at 20 μg/ml concentration decreased Ki67 expressing Tregs by 1.7 fold (p=0.02) compared to the Fc control treatment (Figure 3B). The percentage of total CD4+ T cells remained unchanged between control and ephrin-B2-Fc treated groups (Supplementary Figure 6A). To examine molecular mediators that might be affecting T cell function downstream of EphB4-ephrin-B2, we focused on signaling molecules known to be involved in both T cell signaling and EphB4-ephrin-B2 signaling. Substantial evidence from studies on normal physiology and inflammation suggests that these involve a complex array of signaling pathways, including PI3-Kinase, MEK, STAT3, Src family kinases, and p38 MAPK pathways (35–37), which

have previously been implicated in T cell activation and proliferation (35,36,38). In addition, reports have suggested JAK/STAT as an Eph receptor downstream pathway and we have previously demonstrated that blockade of EphB4-ephrin-B2 signaling combined with RT decreases p-STAT3 in HNSCC tumors (16). Therefore, we examined changes in p-STAT3 in Tregs after ephrin-B2-Fc treatment by flow cytometry. Our data show that 20 μg/ml ephrin-B2-Fc and the PEGylated form of TNYL-RAW similarly decreased STAT3 phosphorylation in Tregs (Figure 3C).

Tregs also constitutively express high levels of IL-2Rα and depend on IL-2 for proliferation, survival and proper functioning. Since we observed decreased Ki67-expressing Tregs following a high dose of ephrin-B2-Fc, we investigated if this may be mediated by reduced secretion of cytokines such as IL-2. Our data indeed show a decrease in the secreted levels of IL-2 (p=0.07) (Figure 3D) as well as of TGF-β (p=0.009) (Figure 3E), a key regulator of Treg function (39), in the conditioned media of Treg cells treated with 20 μg/ml ephrin-B2-Fc. We also performed CIBERSORT analysis on TCGA HNSCC dataset and failed to find any correlation between Foxp3 and EphB4 or ephrin-B2. However, TGF-β, a regulator and mediator of Treg functionality (39) showed some correlation with ephrin-B2/EphB4 in human HNSCC TCGA database on R2 analysis platform (Supplementary figure 6B–C). In addition, decreased levels of pro-survival markers such as p-AKT, and Bcl-XL were observed in T cell lysates by western blotting after 24 hours treatment with the high concentration of ephrin-B2-Fc compared to the control-Fc (Supplementary Figure 6D). The levels of cleaved caspase-3, on the other hand, increased following treatment with 20 μg/ml ephrin-B2-Fc compared to the control-Fc (Supplementary Figure 6D).

Disruption of EphB4-ephrin-B2 signaling combined with radiation generates a potent anti-tumor response in immunocompetent orthotopic HNSCC models

RT remains the mainstay of cancer treatment and is used in combination with chemotherapeutic or targeted agents for the definitive management of HNSCC patients. However, in addition to acting as an adjuvant to immunotherapy, RT also enhances the levels of both EphB4 and ephrin-B2 in Ly2 tumors as shown in Supplementary Figure 7A–B. Therefore, we evaluated the efficacy of combining EphB4-ephrin-B2 inhibitor, TNYL-RAW-Fc, with RT to suppress tumor growth by modulating the tumor immune microenvironment and mitigating the pro-tumorigenic effects of EphB4-ephrin-B2 signaling in the Ly2 orthotopic model. We also compared the *in vivo* efficacy of combined EphB4-ephrin-B2 inhibition and RT with that of combined immune checkpoint inhibitor anti-PDL1 and RT. The experimental design is shown in Figure 4A.

Our data show that radiation alone (RT+IgG+pcDNA3) reduced tumor growth by 2.2 fold (p=0.0003) compared to the IgG+pcDNA3 control group (Figure 4B–D). However, when TNYL-RAW-Fc was used in combination with RT, the combination group resulted in a 4.4 fold reduction compared to TNYL-RAW-Fc alone (p=0.0003) (Figure 4B–D). Importantly, when EphB4-ephrin-B2 inhibition was combined with RT, a similar anti-tumor response was generated as anti-PDL1 combined with RT (Figure 4B–D) at day 20 post-tumor implantation. Triple combination with anti-PDL1+RT and TNYL-RAW-Fc did not add additional synergy (Supplementary Figure 7C–E). Monitoring tumor growth over extended

period of time showed enhanced tumor growth suppression in the RT+IgG+TNYL combination group compared to RT+IgG+pcDNA3 in Ly2 tumors (Supplementary Figure 7C–E). We also evaluated the efficacy of combining TNYL-RAW-Fc inhibitor with RT in another aggressive HNSCC tumor model, Moc2 and it showed similar tumor growth suppression in the combination groups compared to single-agent RT alone (Supplementary Figure 7F–I). Treating Moc2 tumors with RT resulted in a significant 1.59 fold reduction (p<0.0001) in tumor growth compared to the control pcDNA3 group. When TNYL-RAW-Fc inhibitor was combined with RT, it decreased tumor growth by 1.36 fold (p<0.005). The irradiated groups when combined with either TNYL-RAW-Fc or anti-PDL1 resulted in similar level of tumor growth suppression compared to RT alone at day 17 and day 21 post-tumor implantation (Supplementary Figure 7G, H). Similar to the Ly2 model, combining TNYL-RAW-Fc inhibitor with anti-PDL1+RT failed to show any additional benefit (Supplementary Figure 7F–I).

To understand the contribution of EphB4-ephrin-B2 inhibition to immune modulation in the presence of RT, we analyzed Ly2 tumors harvested from the control and TNYL-RAW-Fc groups with and without RT by flow cytometry. Our data demonstrated that in the absence of RT, EphB4-ephrin-B2 inhibition increased CD8+ T cell population (Figure 5A) without affecting the CD4+ T cell subset (Figure 5B). Exposing Ly2 tumors to 10 Gy dose of RT resulted in a significant enhancement of both CD8+ T cells and CD4+ T cells at day 3 post-RT (Figure 5A, B). EphB4-ephrin-B2 inhibition with RT did not affect these T cell populations compared to RT alone (Figure 5A, B). We observed a 1.6 fold decline in the Treg population with RT treatment compared to the control group at day 3 post-RT (p=0.009) (Figure 5C). Addition of TNYL-RAW-Fc to RT resulted in a further decline (~2.7 fold total) in the tumor-infiltrating Tregs compared to both of the single agents (Figure 5C). The CD8+ T cell to Treg ratio was also significantly increased in the combination treatment compared to control or TNYL-RAW-Fc treatment (Figure 5D). To examine the effect of EphB4-ephrin-B2 inhibition with RT on T-cell function, we evaluated the percentage of activated CD8 T cells (CD8+IFNγ+) (Figure 5E) and activated conventional CD4 T cells (CD4+Foxp3-IFNγ+) (Figure 5F). We observed an increase in the percentage of both in the combination group (2.2–2.4 fold) compared to TNYL-RAW-Fc alone. In addition, inhibiting EphB4-ephrin-B2 interaction with RT also resulted in a significant increase in CD4+Foxp3-IFNγ+ cells (2.2 fold) (p=0.04) compared to RT alone (Figure 5F). Increased levels of secreted IP-10/CXCL10, a potent chemokine that attracts functional cytotoxic T cells, was induced by TNYL-RAW-Fc or RT treatment, and further increased by the combination of both treatments compared to RT (Figure 5G). Finally, a 1.4 and 1.8 fold decrease in circulating TGF-β, an output of Tregs' immunosuppressive action, was observed with the TNYL-RAW-Fc and RT treatment, respectively, compared to the control group (Figure 5H). Combining TNYL-RAW-Fc with RT further potentiated the decrease in TGF-β levels (p=0.02 compared to RT) (Figure 5H).

Combined EphB4-ephrin-B2 inhibition and radiation decreases the infiltration of tumor-associated macrophages independently of the effect on T cells

To determine whether the decrease in TAMs is a direct consequence of the changes in Tregs, which are known to promote monocyte differentiation to macrophages, we tested the effect

of EphB4-ephrin-B2 inhibition in nude mice, a T cell independent model. We used HNSCC PDX tumor models known to preserve the tumor environment and mimic human cancers. We have previously shown a significant decrease in tumor growth following EphB4-ephrin-B2 inhibition using sEphB4-HSA in combination with radiation only or radiation and the EGFR inhibitor cetuximab (16,17). sEphB4-HSA is a soluble protein that inhibits the interaction between EphB4 and ephrin-B2 by binding to ephrin-B2 (while TNYL-RAW inhibits the interaction by binding to EphB4) (26). We measured TAM infiltration by using T2 weighted-MRI with iron oxide (SPIO) accumulation in a HNSCC PDX tumor model. We observed that while RT by itself considerably increases SPIO uptake as represented by decreased signal intensity, inhibiting EphB4-ephrin-B2 interaction with sEphB4-HSA reversed this effect of RT (p<0.05) (Supplementary figure 8A, B).

These imaging data were further corroborated by IF staining using CUHN013 tumors harvested from control and experimental groups. This demonstrated that inhibition of EphB4-ephrin B2 with sEphB4-HSA in combination with RT significantly decreases the percentage of TAMs, as determined by the reduction in the staining for the pan-macrophage markers CD107b+ and F4/80+ compared to either treatment alone (Figure 6A–C). We also observed a decrease in the staining for CD163+ M2 macrophages (Figure 6A, D), and an increase in the staining for Gpr18+ M1 macrophages (Figure 6A, E) in CUHN013 tumors, suggesting that EphB4-ephrin-B2 inhibition and RT shift the polarization of macrophages from the pro-tumor M2 phenotype to the anti-tumor M1 phenotype. This is also evident in the increased ratio of M1 to M2 markers (Gpr18:CD163), which is potentiated in the combination group (Figure 6F). Finally, analysis of circulating cytokine/chemokine profiles demonstrates that combining sEphB4-HSA with RT significantly decreases the levels of macrophage colony-stimulating factor (M-CSF), a key differentiation factor that mediates M2 polarization, compared to the single agent treatments (40) (Figure 6G). This is accompanied by a marked increase in the levels of both GM-CSF (Figure 6H) and IFNγ (Figure 6I), particularly in the combination treatment group as compared to either sEphB4-HSA alone or RT alone. Both GM-CSF and IFNγ are known to favor M1 polarization (40). Thus, taken together, our data indicate that combined EphB4-ephrin-B2 inhibition and RT induce an anti-tumor immune response by affecting macrophage polarization.

A low M1/M2 ratio correlates with poor survival and disease-free survival in HNSCC

In light of our data showing that EphB4-ephrin-B2 inhibition favors a polarization towards an M1 phenotype, we performed TCGA and CIBERSORT analysis to examine the significance of such polarization on the survival of HNSCC patients. Our analysis revealed for the first time that a significant correlation exists between lower M1/M2 ratio and poor overall survival as well as disease-free survival (Supplementary figure 8C, D). The analysis was based on a cut-off M1/M2 ratio of 0.5. When the M1/M2 ratio is < 0.5, patients have poor overall survival rates compared to patients with M1/M2 ratio > 0.5. The median survival for patients with M1/M2 ratio > 0.5 was 65.8 months compared to 32.8 months (p=0.0170) for patients with M1/M2 ratio < 0.5 (Supplementary figure 8C). Furthermore, the median time to disease progression in patient cohort with M1/M2 ratio > 0.5 was 76.2 months compared to 53.1 months (p=0.0111) for patients with < 0.5 M1/M2 ratio (Supplementary figure 8D). When we interrogated the HNSCC datasets, we observed no

correlation between EphB4 or ephrin-B2 expression and composite M2-related macrophages. Some positive correlation was however evident between ephrin-B2 and M2 marker-HRH1 (Supplementary figure 8E–F).

Discussion

The advent of immunotherapy has shown promising outcomes in several disease models, albeit the response rates have been sub-optimal (41). In addition, immune-related adverse toxicity and development of resistance poses a major hurdle that compromises the efficacy of immunotherapeutic agents (5,42). Thus, it is important to search for alternate therapeutic strategies that can remodel the tumor immune microenvironment to generate a potent anti-tumor immune response.

Multiple pieces of evidence show that EphB4-ephrin-B2 interaction regulates different immune cell processes, including proliferation, survival, apoptosis, activation, and migration (22,23,34,38). The reported effects vary in different studies, possibly due to different levels of blockade of Eph receptor-ligand interaction (23,34,38). A report by Kawano *et al.*, examined the total CD3 T cell population without distinguishing between different subset of T cells, making it challenging to appreciate the full spectrum of the biological impact of EphB4-ephrin-B2 signaling (34). Our data are the first to show a differential effect of EphB4-ephrin-B2 blockade on different T cell populations in a HNSCC model, with selective targeting of Tregs.

Tregs present in the TME act as one of the major immunosuppressors, dampening the activity of Teffector cells and immunotherapy-induced anti-tumor responses (5). The outcome of an anti-tumor immune response depends on the balance between the activities of intratumoral Teffector cells and immune suppressive cell populations, including Tregs. Our data show that the decrease in Tregs observed with inhibition of EphB4-ephrin-B2 interaction in orthotopic HNSCC models is associated with increased activation of the CD8+ and CD4+Foxp3- conventional CD4 T cells known to be involved in anti-tumor immune response. In addition, increased T cell activation is also inferred with EphB4-ephrin-B2 inhibition combined with RT, based on the increased circulating plasma levels of IP-10/CXCL10, which is a member of the CXC chemokine family that binds to the CXCR3 receptor on Teffector cells to enhance chemotaxis, activation, growth, and angiostatic effects (43). In contrast, the levels of circulating TGF-β1, a master regulator of Treg function (39), were significantly reduced by the combination of EphB4-ephrin-B2 inhibition and RT. In addition to its effects on T cell subsets, EphB4-ephrin-B2 inhibition also increased the dendritic cell population, which is known to be involved in antigen presentation. These data are in agreement with a report demonstrating that Tregs cross-talk with intratumoral dendritic cells to suppress an activated T cell response and that Treg ablation in turn results in an effective anti-tumor response by restoring immunogenic CD11C+ dendritic cells and activating the CD8+ T cell population (44). Our results are also concordant with what is known for functional roles of receptor tyrosine kinases. Several studies have reported that AXL, another tyrosine receptor kinase similar in structure and function to EphB4, has effects on both cancer cell as well as immune cells (45,46). AXL inhibition has been shown

to induce an anti-tumor immune response in syngeneic ovarian cancer and lung cancer models (45).

The impact of Tregs in HNSCCs has been a controversial topic (47–50). While a positive correlation between Tregs and prognosis has been reported in a meta-analysis in HNSCCs (47), it is important to note that the data presented are highly heterogenous and the study only focused on univariate analysis of the results. In a study by Mandal *et al.* (48), such prognostic significance of Tregs was lost on multivariate analysis after adjustment for other immune cells. These results indicate that Treg levels in HNSCC co-vary with broader trends among T cell populations, and that Treg levels in isolation may not represent the overall net level of immune activation or suppression in the TME. Supportive of a role of Tregs in driving resistance to treatment are also results from a cross sectional study showing that in the setting of postoperative chemoradiation, Tregs were increased in frequency and persisted afterwards especially in those with active disease and could be responsible for suppression of anti-tumor immune responses and recurrence in HNSCC (50). Consistent with these findings, Hanna *et al.* (49), demonstrated a correlation between an inflamed tumor subtype in the recurrent, metastatic squamous cell carcinoma with improved survival compared with a non-inflamed subtype characterized by low CD8+ T cells, low PD-1/TIM3 co-expression, and higher Tregs.

The mechanisms of how Tregs suppress Teffector function and how EphB4-ephrin-B2 interaction contributes to this effect remain a subject of investigation. Our *in vitro* data show that inhibition of EphB4-ephrin-B2 function decreases Ki67+Tregs and decreases circulating IL-2. The contribution of baseline peripheral Ki67+ Tregs in response to immunotherapy has been recently shown to be directly, and unexpectedly, a positive correlation. In an analysis of CheckMate141 trial, baseline Ki67+ Treg levels were found to be lower in non-responders whereas PD-1+Treg population was significantly reduced following nivolumab (anti-PD1 antibody) treatment in both responders and non-responders (51). While these data might seem counterintuitive, and they only apply to baseline circulatory levels which may or may not reflect the dynamics of the TME, they nevertheless highlight an important unmet need in terms of understanding of Treg biology. An elegant study by Maj *et al.*, 2017 (52), has shown that all Tregs within the ovarian cancer TME express high Ki67. But it is the apoptotic Tregs, induced by a highly acidic and hypoxic TME, that mediate that mediate immunosuppression via the adenosine pathway (52). Others have argued that Tregs suppress Teffectors by consumption of IL-2 thus forcing Teffectors to undergo lymphokine withdrawal apoptosis (53). Our data support a decrease in Ki67+ Tregs and total numbers of Tregs upon TNYL-RAW mediated EphB4-ephrinB2 inhibition along with a decrease in circulating IL2 levels. We observe an increase in CD8 T cell activation status, which we believe is due to direct removal of Treg immunosuppression. However, the exact mechanisms of how EphB4-ephrin-B2 inhibition might be influencing Tregs immunosuppressive activity on Teffectors remain unclear. We are employing conditional knockouts of EphB4 and ephrin-B2 for a more in-depth understanding of the mechanisms by which the interaction of the EphB4 receptor with its cognate ligand affects the immune microenvironment in the TME. This along with human samples from clinical trials employing EphB4-ephrin-B2 inhibitors in HNSCCs should improve such understanding.

Using the R2 analysis on HNSCC datasets, we found EphB4 and ephrin-B2 levels to correlate with TGF-β, a regulator and mediator of Treg function (39), as well as HRH1-a mediator of M2 function (54). No specific correlation was found between either EphB4 or ephrin-B2 and Foxp3 or composite M2 markers in our CIBERSORT TCGA analyses. These data, however, have to be interpreted with caution. First, CD25 is not included in the CIBERSORT analysis so the validity of defining a "Treg" population remains to be established using this approach. Second, correlating gene expressions with immune signatures in the TCGA analysis remains a challenge, particularly for genes richly expressed on the stroma. This has been attributed to tumor purity (55), where the presence of non-tumor cell populations such as immune cells, endothelial, and stromal cells in the surgical specimens can skew the analyses of cancer gene expression profiles. It should be further noted that such tumor purity can act as a key confounding factor when deducing correlation between gene expression, mutational burden, gene clustering, and molecular taxonomy and should be taken into consideration (55). We know based on our data that ephrin-B2 is present on some cancer cells and stroma while EphB4 is present both on cancer cells and stroma including Tregs. This calls into question the validity of such data and awaits confirmation by flow cytometry in future clinical trials.

Whether the increase in the CD8 T cell/Treg ratio induced by TNYL-RAW-Fc is intratumoral or systemic is an important distinction in light of the published literature showing the role of EphB4-ephrin-B2 in regulating mobilization of hematopoietic stem and progenitor cells from the bone marrow (24). Using genetically engineered mouse models as well as subcutaneous ovarian and breast cancer mouse xenograft models, Kwak *et al.* showed that EphB4 regulates transendothelial migration of hematopoietic stem/progenitor cells from bone marrow sinusoids, and that EphB4-ephrin-B2 inhibition decreases both blood and tumor infiltrating hematopoietic stem/progenitor cells and thus tumor growth (24). In contrast, we did not observe changes in circulating lymphocytes, suggesting that the effect is likely exerted intratumorally. During development, ephrin-B ligands were also recently demonstrated to act on T cell homing by blocking their recruitment and retention *via* chemorepulsive interactions with EphB-receptor-expressing Teffector cells in germinal centers (56). This is not surprising in view of the previous report by Korff *et al.* (57), suggesting that ephrin-B2 is expressed on the luminal surface of resting endothelial cells and EphB receptors are present on circulating leukocytes.

The mechanisms by which EphB4-ephrin-B2 interaction alters T cell numbers and function remain poorly understood. Suppression of T cell function has been demonstrated for Eph/ephrin family members (22,23,35). Inhibition of CD4+ T cell proliferation has been previously demonstrated in response to ephrin-A1 signaling (22), a process that is likely mediated by activation of Src-family kinases, AKT phosphorylation, and T cell apoptosis blockade (35). Other signaling pathways such as MEK, STAT3, and p38 MAPK have also been implicated in T cell activation and proliferation (35,36,38). EphB4-ephrin-B2 interaction between mesenchymal stem cells and T cells can also suppress T cell proliferation (23). Conflicting data, however, also suggest that the Eph/ephrin system can stimulate T cell function (58,59). These functional contradictions could be explained by the concentration of available ligand that might result in different responses on T cells. A recent study showed that the involvement of ephrin-B1 and ephrin-B2 in T cell proliferation is dose

dependent (34), whereby low doses enhanced CD3-mediated murine T cell proliferation and an opposite effect was observed at higher doses (34). Our data show that at high concentration, ephrin-B2-Fc decreases Ki67-expressing Treg population. In addition, we also observed a decrease in the levels of p-AKT and BCL-XL in T cells at high ephrin-B2-Fc concentration similar to what has been previously reported (34–38).

Another immune cell population that has emerged as a main target of EphB4-ephrin-B2 inhibition are the tumor-associated macrophages (TAMs). Overexpression of EphB4 on monocytes has also been shown to augment monocyte adhesion (21). In atherosclerosis, it was shown that endothelial ephrin-B2 activates the EphB2 receptor on monocytes and induces cytokine expression in monocytes (18). In this study, we show that inhibition of the interaction between EphB4 and ephrin-B2 causes a significant reduction in TAMs. While a decrease in intratumoral myeloid cells has been shown before with EphB4-ephrin-B2 inhibition and attributed to decreased exit of hematopoietic stem and progenitor cells from the bone marrow (24), in our HNSCC tumor models we show a specific decrease of pro-tumoral M2 macrophages compared to the anti-tumoral M1 macrophages. Our TCGA analysis further shows that the M1/M2 ratio is a prognostic predictor of both disease-free survival and overall survival in the HNSCC patient population. Our data is in concordance with the published reports suggesting that polarization of TAMs toward a M2 phenotype, indicated by a lower M1/M2 ratio predicts for poor response to chemoradiation and shorter survival in locally advanced cervical cancer (60). The polarization of TAMs toward M1 phenotype upon inhibition of EphB4-ephrin-B2 is most evident when combined with RT. In oral cavity cancers, the recolonization of tumors by M2-like macrophages post-RT has also been shown to elicit the secretion of pro-angiogenic factors that contribute to neo-angiogenesis, favoring tumor regrowth (61). In our HNSCC model, we show that the combined treatment with an EphB4-ephrin-B2 inhibitor and RT decreases macrophages with the M2 phenotype.

Radiation therapy remains the standard of care treatment in the definitive management of patients with locally advanced HNSCCs and can act as an adjuvant for immunotherapy but there are some undesirable effects mounted in response to RT that in turn compromises the efficacy of immunotherapeutic agents. RT is unable to overcome the accumulation of immunosuppressive populations such as Tregs in the later (repair) phase (5). Therefore, finding other treatments that synergize with RT and counteract its negative effects is critical to overcome adverse side-effects, treatment resistance, and tumor regrowth. In addition, we observed that RT upregulates EphB4 and EFNB2 mRNA levels in murine Ly2 tumors particularly in the late phase of tumor regrowth. Therefore, combining RT with EphB4-EFNB2 inhibitor (TNYL-RAW-Fc) provides rationale in mitigating the undesirable pro-tumor effects triggered as a result of EphB4-EFNB2 signaling. Our data demonstrate that inhibiting EphB4-ephrin-B2 signaling using TNYL-RAW-Fc significantly enhances the radiosensitivity of Ly2 tumors and suppresses tumor growth. Combining TNYL-RAW with RT counteracts the negative influence of RT by further inhibiting Tregs and M2 macrophages and resulting in an effective anti-tumor immune response, enhanced cytotoxic T cell function, and tumor growth suppression. It is also interesting to note that the magnitude of tumor reduction following TNYL-RAW-Fc administration with RT is similar to immune checkpoint inhibitor (anti-PDL1 antibody) combined with RT particularly at

early time-points. We further investigated whether combining EphB4-ephrin-B2 inhibitor with Anti-PDL1+RT can generate synergistic response but we failed to observe any enhanced benefit in the triple combination group in terms of tumor growth reduction in both Ly2 and Moc2 tumor models suggesting that alternate tumor growth promoting pathways such as EGFR that might be involved in cross-talk with EphB4-ephrin-B2. This further suggests that combined blockade of these two pathways might elicit a more effective anti-tumor response. This is not surprising in view of the fact that EGFR-targeted agents have been shown to induce tumor regression by stimulating tumor-specific immune responses (62) and warrants further scrutiny in our tumor models. Nonetheless, our study provides supportive evidence suggesting that EphB4-ephrin-B2 blockade with RT alters both innate and adaptive arms of the immune system as demonstrated in both immunocompetent and PDX HNSCC models using two different inhibitors targeting the EphB4-ephrin-B2 axis.

Overall, our study is the first report demonstrating the novel role of EphB4-ephrin-B2 interaction in remodeling the tumor immune microenvironment in HNSCC. Our findings offer a potential alternative in the form of EphB4-ephrin-B2 targeted therapeutics that can be tested in clinical trials in combination with RT for the treatment of HNSCC patients.

Supplementary Material

Refer to Web version on PubMed Central for supplementary material.

Acknowledgements

References

1. Szturz P, Vermorken JB. Immunotherapy in head and neck cancer: aiming at EXTREME precision. BMC Med 2017;15:110 [PubMed: 28571578]

2. Ferris RL, Blumenschein G Jr., Fayette J, Guigay J, Colevas AD, Licitra L, et al. Nivolumab vs investigator's choice in recurrent or metastatic squamous cell carcinoma of the head and neck: 2-year long-term survival update of CheckMate 141 with analyses by tumor PD-L1 expression. Oral Oncol 2018;81:45–51 [PubMed: 29884413]

3. Chow LQM, Haddad R, Gupta S, Mahipal A, Mehra R, Tahara M, et al. Antitumor Activity of Pembrolizumab in Biomarker-Unselected Patients With Recurrent and/or Metastatic Head and Neck Squamous Cell Carcinoma: Results From the Phase Ib KEYNOTE-012 Expansion Cohort. J Clin Oncol 2016;34:3838–45 [PubMed: 27646946]

4. Siu LL, Even C, Mesia R, Remenar E, Daste A, Delord JP, et al. Safety and Efficacy of Durvalumab With or Without Tremelimumab in Patients With PD-L1-Low/Negative Recurrent or Metastatic HNSCC: The Phase 2 CONDOR Randomized Clinical Trial. JAMA Oncol 2018

5. Oweida A, Hararah MK, Phan A, Binder D, Bhatia S, Lennon S, et al. Resistance to Radiotherapy and PD-L1 Blockade Is Mediated by TIM-3 Upregulation and Regulatory T-Cell Infiltration. Clin Cancer Res 2018

6. Mei J, Xiao Z, Guo C, Pu Q, Ma L, Liu C, et al. Prognostic impact of tumor-associated macrophage infiltration in non-small cell lung cancer: A systemic review and meta-analysis. Oncotarget 2016;7:34217–28 [PubMed: 27144518]

7. Jie HB, Gildener-Leapman N, Li J, Srivastava RM, Gibson SP, Whiteside TL, et al. Intratumoral regulatory T cells upregulate immunosuppressive molecules in head and neck cancer patients. Br J Cancer 2013;109:2629–35 [PubMed: 24169351]

8. Olson OC, Kim H, Quail DF, Foley EA, Joyce JA. Tumor-Associated Macrophages Suppress the Cytotoxic Activity of Antimitotic Agents. Cell Rep 2017;19:101–13 [PubMed: 28380350]

9. Arce Vargas F, Furness AJS, Solomon I, Joshi K, Mekkaoui L, Lesko MH, et al. Fc-Optimized Anti-CD25 Depletes Tumor-Infiltrating Regulatory T Cells and Synergizes with PD-1 Blockade to Eradicate Established Tumors. Immunity 2017;46:577–86 [PubMed: 28410988]

10. Robert C, Schachter J, Long GV, Arance A, Grob JJ, Mortier L, et al. Pembrolizumab versus Ipilimumab in Advanced Melanoma. N Engl J Med 2015;372:2521–32 [PubMed: 25891173]

11. Pasquale EB. Eph-ephrin bidirectional signaling in physiology and disease. Cell 2008;133:38–52 [PubMed: 18394988]

12. Ferguson BD, Tretiakova MS, Lingen MW, Gill PS, Salgia R. Expression of the EPHB4 receptor tyrosine kinase in head and neck and renal malignancies--implications for solid tumors and potential for therapeutic inhibition. Growth Factors 2014;32:202–6 [PubMed: 25391996]

13. Masood R, Kumar SR, Sinha UK, Crowe DL, Krasnoperov V, Reddy RK, et al. EphB4 provides survival advantage to squamous cell carcinoma of the head and neck. Int J Cancer 2006;119:1236–48 [PubMed: 16615113]

14. Oweida A, Bhatia S, Hirsch K, Calame D, Griego A, Keysar S, et al. Ephrin-B2 overexpression predicts for poor prognosis and response to therapy in solid tumors. Mol Carcinog 2017;56:1189–96 [PubMed: 27649287]

15. El-Khoueiry BG A, Cole S, Tsao-Wei D, Goldkorn A, Quinn D, Lenz HJ, Nieva J, Dorff T, Oswald M, Berg J, Menendez X, Karakozian K, Krasnoperov V, Liu R, Thomas J, Groshen S, Gill P. A first-in-human phase I study of sEphB4-HSA in patients with advanced solid tumors with expansion at the maximum tolerated dose (MTD) or recommended phase II dose (RP2D). Eur J Cancer 2016;69

16. Bhatia S, Hirsch K, Sharma J, Oweida A, Griego A, Keysar S, et al. Enhancing radiosensitization in EphB4 receptor-expressing Head and Neck Squamous Cell Carcinomas. Sci Rep 2016;6:38792 [PubMed: 27941840]

17. Bhatia S, Sharma J, Bukkapatnam S, Oweida A, Lennon S, Phan A, et al. Inhibition of EphB4-Ephrin-B2 Signaling Enhances Response to Cetuximab-Radiation Therapy in Head and Neck Cancers. Clin Cancer Res 2018;24:4539–50 [PubMed: 29848571]

18. Braun J, Hoffmann SC, Feldner A, Ludwig T, Henning R, Hecker M, et al. Endothelial cell ephrinB2-dependent activation of monocytes in arteriosclerosis. Arterioscler Thromb Vasc Biol 2011;31:297–305 [PubMed: 21127290]

19. Poitz DM, Ende G, Stutz B, Augstein A, Friedrichs J, Brunssen C, et al. EphrinB2/EphA4-mediated activation of endothelial cells increases monocyte adhesion. Mol Immunol 2015;68:648–56 [PubMed: 26552760]

20. Funk SD, Yurdagul A Jr., Albert P, Traylor JG Jr., Jin L, Chen J, et al. EphA2 activation promotes the endothelial cell inflammatory response: a potential role in atherosclerosis. Arterioscler Thromb Vasc Biol 2012;32:686–95 [PubMed: 22247258]

21. Pfaff D, Heroult M, Riedel M, Reiss Y, Kirmse R, Ludwig T, et al. Involvement of endothelial ephrin-B2 in adhesion and transmigration of EphB-receptor-expressing monocytes. J Cell Sci 2008;121:3842–50 [PubMed: 18957513]

22. Wohlfahrt JG, Karagiannidis C, Kunzmann S, Epstein MM, Kempf W, Blaser K, et al. Ephrin-A1 suppresses Th2 cell activation and provides a regulatory link to lung epithelial cells. J Immunol 2004;172:843–50 [PubMed: 14707054]

23. Nguyen TM, Arthur A, Hayball JD, Gronthos S. EphB and Ephrin-B interactions mediate human mesenchymal stem cell suppression of activated T-cells. Stem Cells Dev 2013;22:2751–64 [PubMed: 23711177]

24. Kwak H, Salvucci O, Weigert R, Martinez-Torrecuadrada JL, Henkemeyer M, Poulos MG, et al. Sinusoidal ephrin receptor EPHB4 controls hematopoietic progenitor cell mobilization from bone marrow. J Clin Invest 2016;126:4554–68 [PubMed: 27820703]

25. Noberini R, Mitra S, Salvucci O, Valencia F, Duggineni S, Prigozhina N, et al. PEGylation potentiates the effectiveness of an antagonistic peptide that targets the EphB4 receptor with nanomolar affinity. PLoS One 2011;6:e28611 [PubMed: 22194865]

26. Koolpe M, Burgess R, Dail M, Pasquale EB. EphB receptor-binding peptides identified by phage display enable design of an antagonist with ephrin-like affinity. J Biol Chem 2005;280:17301–11 [PubMed: 15722342]

27. Serkova NJ, Renner B, Larsen BA, Stoldt CR, Hasebroock KM, Bradshaw-Pierce EL, et al. Renal inflammation: targeted iron oxide nanoparticles for molecular MR imaging in mice. Radiology 2010;255:517–26 [PubMed: 20332377]

28. Oweida A, Lennon S, Calame D, Korpela S, Bhatia S, Sharma J, et al. Ionizing radiation sensitizes tumors to PD-L1 immune checkpoint blockade in orthotopic murine head and neck squamous cell carcinoma. Oncoimmunology 2017;6:e1356153 [PubMed: 29123967]

29. Casella G, Garzetti L, Gatta AT, Finardi A, Maiorino C, Ruffini F, et al. IL4 induces IL6-producing M2 macrophages associated to inhibition of neuroinflammation in vitro and in vivo. J Neuroinflammation 2016;13:139 [PubMed: 27266518]

30. Ying W, Cheruku PS, Bazer FW, Safe SH, Zhou B. Investigation of macrophage polarization using bone marrow derived macrophages. J Vis Exp 2013

31. Cancer Genome Atlas Research N, Weinstein JN, Collisson EA, Mills GB, Shaw KR, Ozenberger BA, et al. The Cancer Genome Atlas Pan-Cancer analysis project. Nat Genet 2013;45:1113–20 [PubMed: 24071849]

32. Newman AM, Liu CL, Green MR, Gentles AJ, Feng W, Xu Y, et al. Robust enumeration of cell subsets from tissue expression profiles. Nat Methods 2015;12:453–7 [PubMed: 25822800]

33. Wikenheiser DJ, Stumhofer JS. ICOS Co-Stimulation: Friend or Foe? Front Immunol 2016;7:304 [PubMed: 27559335]

34. Kawano H, Katayama Y, Minagawa K, Shimoyama M, Henkemeyer M, Matsui T. A novel feedback mechanism by Ephrin-B1/B2 in T-cell activation involves a concentration-dependent switch from costimulation to inhibition. Eur J Immunol 2012;42:1562–72 [PubMed: 22622783]

35. Holen HL, Shadidi M, Narvhus K, Kjosnes O, Tierens A, Aasheim HC. Signaling through ephrin-A ligand leads to activation of Src-family kinases, Akt phosphorylation, and inhibition of antigen receptor-induced apoptosis. J Leukoc Biol 2008;84:1183–91 [PubMed: 18593733]

36. Sharfe N, Freywald A, Toro A, Roifman CM. Ephrin-A1 induces c-Cbl phosphorylation and EphA receptor down-regulation in T cells. J Immunol 2003;170:6024–32 [PubMed: 12794130]

37. Gu C, Park S. The EphA8 receptor regulates integrin activity through p110gamma phosphatidylinositol-3 kinase in a tyrosine kinase activity-independent manner. Mol Cell Biol 2001;21:4579–97 [PubMed: 11416136]

38. Kim I, Ryu YS, Kwak HJ, Ahn SY, Oh JL, Yancopoulos GD, et al. EphB ligand, ephrinB2, suppresses the VEGF- and angiopoietin 1-induced Ras/mitogen-activated protein kinase pathway in venous endothelial cells. FASEB J 2002;16:1126–8 [PubMed: 12039842]

39. Chen W, Jin W, Hardegen N, Lei KJ, Li L, Marinos N, et al. Conversion of peripheral CD4+CD25-naive T cells to CD4+CD25+ regulatory T cells by TGF-beta induction of transcription factor Foxp3. J Exp Med 2003;198:1875–86 [PubMed: 14676299]

40. Samaniego R, Palacios BS, Domiguez-Soto A, Vidal C, Salas A, Matsuyama T, et al. Macrophage uptake and accumulation of folates are polarization-dependent in vitro and in vivo and are regulated by activin A. J Leukoc Biol 2014;95:797–808 [PubMed: 24399840]

41. Postow MA. Managing immune checkpoint-blocking antibody side effects. Am Soc Clin Oncol Educ Book 2015:76–83 [PubMed: 25993145]

42. Maughan BL, Bailey E, Gill DM, Agarwal N. Incidence of Immune-Related Adverse Events with Program Death Receptor-1- and Program Death Receptor-1 Ligand-Directed Therapies in Genitourinary Cancers. Front Oncol 2017;7:56 [PubMed: 28421161]

43. Mukaida N, Sasaki S, Baba T. Chemokines in cancer development and progression and their potential as targeting molecules for cancer treatment. Mediators Inflamm 2014;2014:170381 [PubMed: 24966464]

44. Jang JE, Hajdu CH, Liot C, Miller G, Dustin ML, Bar-Sagi D. Crosstalk between Regulatory T Cells and Tumor-Associated Dendritic Cells Negates Anti-tumor Immunity in Pancreatic Cancer. Cell Rep 2017;20:558–71 [PubMed: 28723561]

45. Guo Z, Li Y, Zhang D, Ma J. Axl inhibition induces the antitumor immune response which can be further potentiated by PD-1 blockade in the mouse cancer models. Oncotarget 2017;8:89761–74 [PubMed: 29163786]

46. Brand TM, Iida M, Stein AP, Corrigan KL, Braverman CM, Coan JP, et al. AXL Is a Logical Molecular Target in Head and Neck Squamous Cell Carcinoma. Clin Cancer Res 2015;21:2601–12 [PubMed: 25767293]

47. de Ruiter EJ, Ooft ML, Devriese LA, Willems SM. The prognostic role of tumor infiltrating T-lymphocytes in squamous cell carcinoma of the head and neck: A systematic review and meta-analysis. Oncoimmunology 2017;6:e1356148 [PubMed: 29147608]

48. Mandal R, Senbabaoglu Y, Desrichard A, Havel JJ, Dalin MG, Riaz N, et al. The head and neck cancer immune landscape and its immunotherapeutic implications. JCI Insight 2016;1:e89829 [PubMed: 27777979]

49. Hanna GJ, Liu H, Jones RE, Bacay AF, Lizotte PH, Ivanova EV, et al. Defining an inflamed tumor immunophenotype in recurrent, metastatic squamous cell carcinoma of the head and neck. Oral Oncol 2017;67:61–9 [PubMed: 28351582]

50. Schuler PJ, Harasymczuk M, Schilling B, Saze Z, Strauss L, Lang S, et al. Effects of adjuvant chemoradiotherapy on the frequency and function of regulatory T cells in patients with head and neck cancer. Clin Cancer Res 2013;19:6585–96 [PubMed: 24097865]

51. Concha-Benavente FGM, Blumenschein GR, Harrington K, Fayette J, Colevas AD, Licitra L, Kasper S, Even C, Worden FP, Saba NF, Haddad RI, Tahara M, Hasegawa Y, Yen CJ, Lynch MJ, Monga M, Geese WJ, Vokes EE, and Ferris RL. Characterization of potential predictive biomarkers of response to nivolumab in CheckMate 141 in patients with squamous cell carcinoma of the head and neck (SCCHN). Journal of Clinical Oncology 2017;35:15_suppl:6050-

52. Maj T, Wang W, Crespo J, Zhang H, Wang W, Wei S, et al. Oxidative stress controls regulatory T cell apoptosis and suppressor activity and PD-L1-blockade resistance in tumor. Nat Immunol 2017;18:1332–41 [PubMed: 29083399]

53. Pandiyan P, Zheng L, Lenardo MJ. The molecular mechanisms of regulatory T cell immunosuppression. Front Immunol 2011;2:60 [PubMed: 22566849]

54. Wang HW, Joyce JA. Alternative activation of tumor-associated macrophages by IL-4: priming for protumoral functions. Cell Cycle 2010;9:4824–35 [PubMed: 21150330]

55. Rhee JK, Jung YC, Kim KR, Yoo J, Kim J, Lee YJ, et al. Impact of Tumor Purity on Immune Gene Expression and Clustering Analyses across Multiple Cancer Types. Cancer Immunol Res 2018;6:87–97 [PubMed: 29141981]

56. Lu P, Shih C, Qi H. Ephrin B1-mediated repulsion and signaling control germinal center T cell territoriality and function. Science 2017;356

57. Korff T, Dandekar G, Pfaff D, Fuller T, Goettsch W, Morawietz H, et al. Endothelial ephrinB2 is controlled by microenvironmental determinants and associates context-dependently with CD31. Arterioscler Thromb Vasc Biol 2006;26:468–74 [PubMed: 16357318]

58. Luo H, Yu G, Wu Y, Wu J. EphB6 crosslinking results in costimulation of T cells. J Clin Invest 2002;110:1141–50 [PubMed: 12393850]

59. Luo H, Yu G, Tremblay J, Wu J. EphB6-null mutation results in compromised T cell function. J Clin Invest 2004;114:1762–73 [PubMed: 15599401]

60. Petrillo M, Zannoni GF, Martinelli E, Pedone Anchora L, Ferrandina G, Tropeano G, et al. Polarisation of Tumor-Associated Macrophages toward M2 Phenotype Correlates with Poor

Response to Chemoradiation and Reduced Survival in Patients with Locally Advanced Cervical Cancer. PLoS One 2015;10:e0136654 [PubMed: 26335330]

61. Okubo M, Kioi M, Nakashima H, Sugiura K, Mitsudo K, Aoki I, et al. M2-polarized macrophages contribute to neovasculogenesis, leading to relapse of oral cancer following radiation. Sci Rep 2016;6:27548 [PubMed: 27271009]

62. Yang X, Zhang X, Mortenson ED, Radkevich-Brown O, Wang Y, Fu YX. Cetuximab-mediated tumor regression depends on innate and adaptive immune responses. Mol Ther 2013;21:91–100 [PubMed: 22990672]

Significance:

Findings present EphB4-ephrin-B2 inhibition as an alternative to anti-PDL1 therapeutics that can be used in combination with radiation to induce an effective anti-tumor immune response in HNSCC patients.
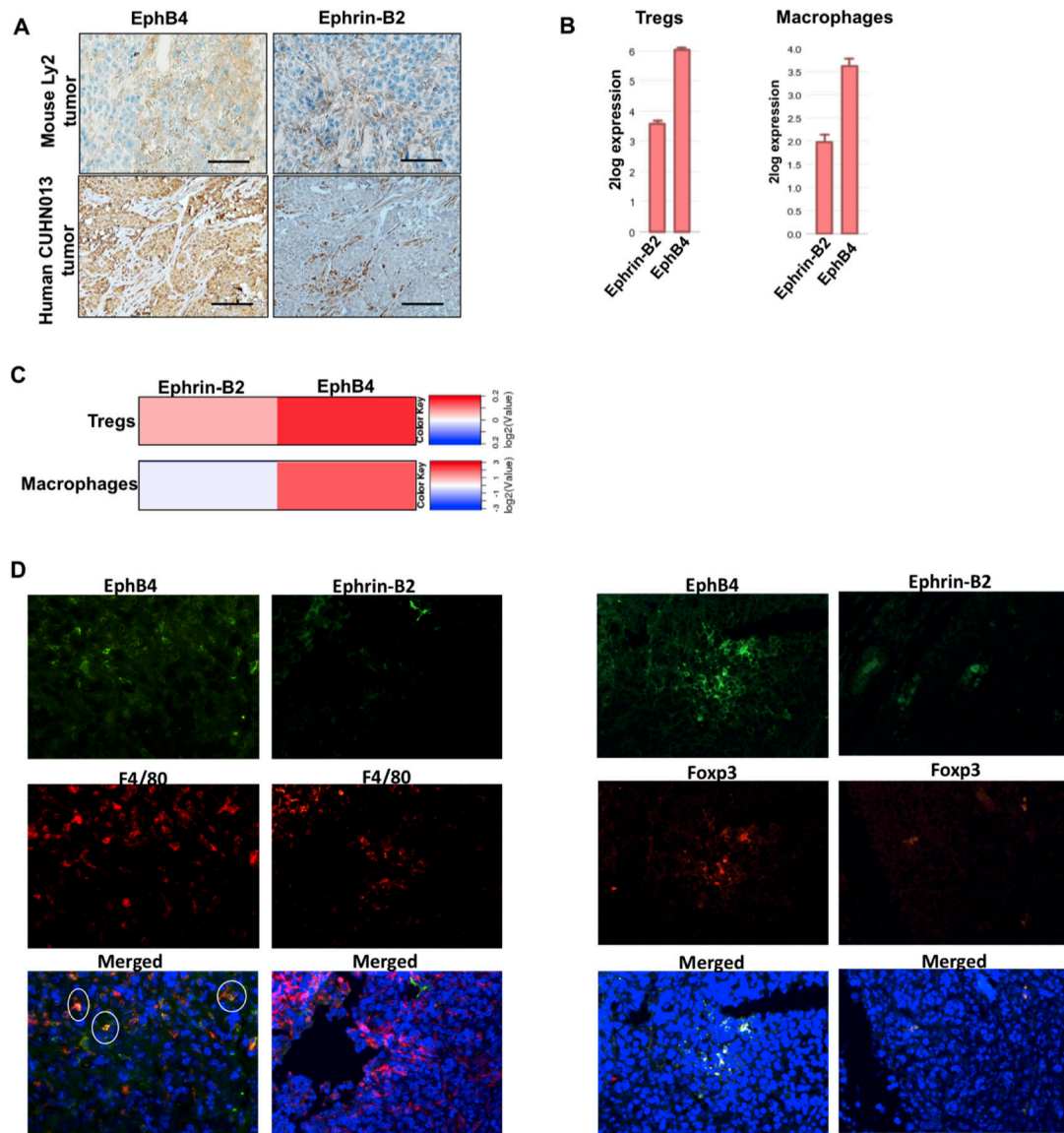
Figure 1. EphB4 is expressed in HNSCC tumor cells, and is present at elevated levels in both Tregs and macrophages compared to ephrin-B2.

IHC analysis was performed on Ly2 tumor sections and CUHN013 human tumors **(A)** and data show the presence of EphB4 on cancer cells and stroma while ephrin-B2 was present on some cancer cells and on stroma. Scale bar: 100 μm. Analysis of Wicker dataset and Salazer dataset show high levels of EphB4 *versus* ephrin-B2 on Tregs and macrophages respectively **(B)**. Analysis of the ImmGen database also shows high expression of EphB4 in Tregs and macrophages compared to ephrin-B2 **(C)**. IF staining showing co-localization of Foxp3 (Treg marker) and F4/80 (macrophage marker) with EphB4 or ephrin-B2 in Ly2 tumors **(D).** Total magnification=200x.
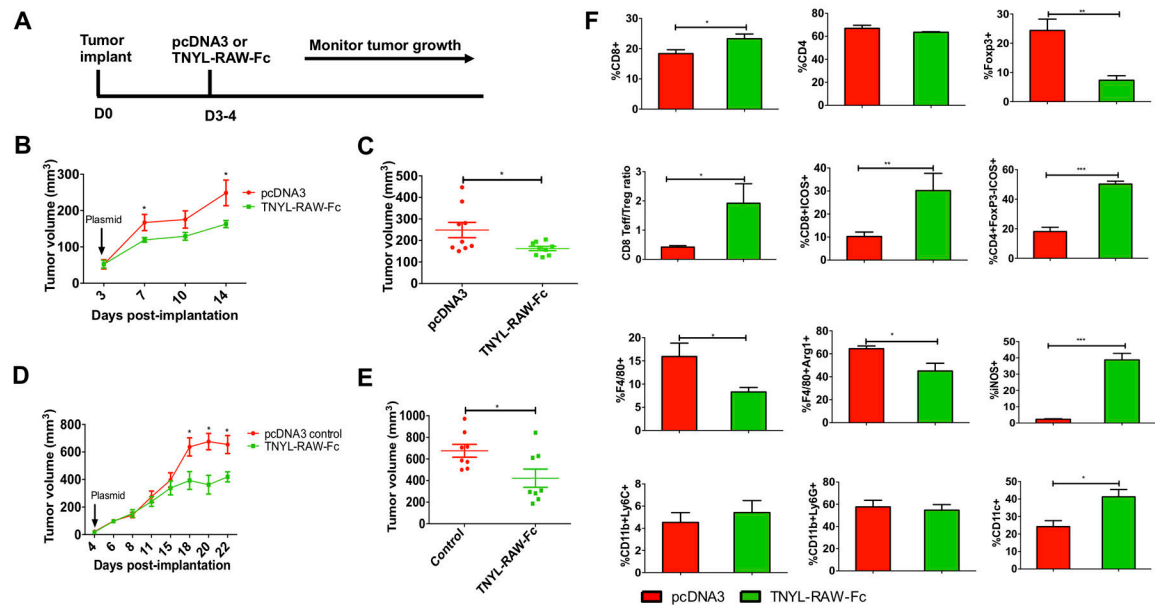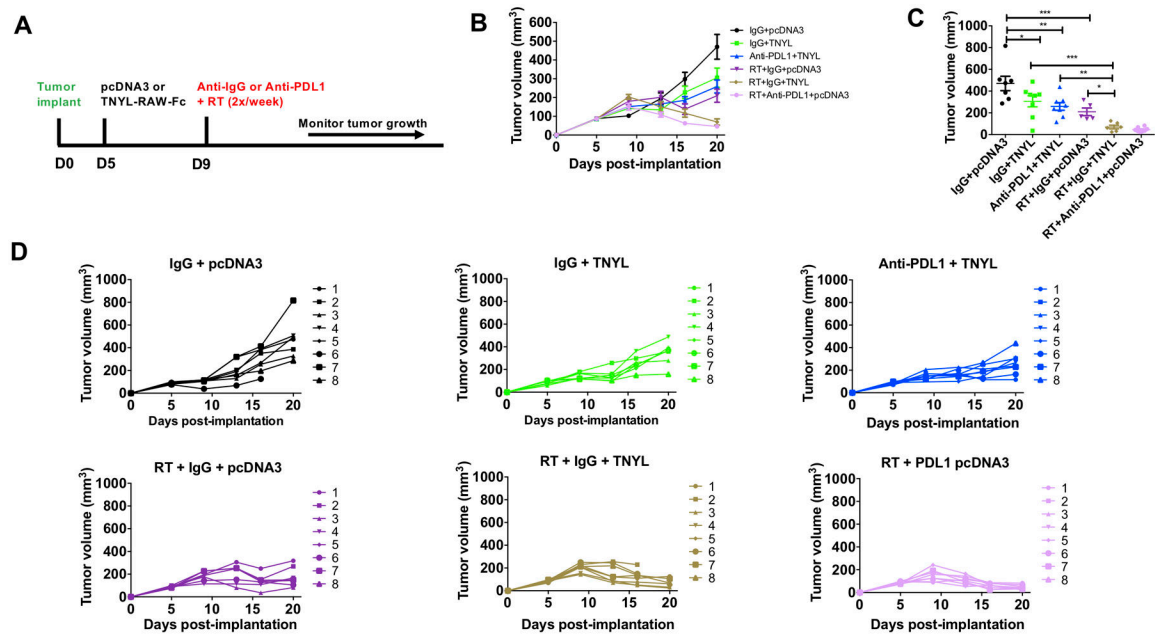
Figure 2. Inhibition of EphB4-ephrin-B2 by TNYL-RAW-Fc results in a significant tumor growth reduction, decreased intratumoral Tregs and TAMs, and increased T cell activation in orthotopic HNSCC models.

The experimental design is shown in **A.** Blockade of EphB4-ephrin-B2 in mice hydrodynamically injected with the TNYL-RAW-Fc plasmid (20 μg/mouse) results in a significant decrease in tumor growth in Ly2 **(B and C)** and Moc2 **(D and E)** tumor-bearing mice. Ly2 tumors from mice treated with either pcDNA3 or TNYL-RAW-Fc plasmids were harvested 11 to 18 days after plasmid administration. Tumors were processed and subjected to mass cytometry analysis. Bar diagrams show quantitative differences in tumor-infiltrating population of immune cells labeled with the indicated markers following TNYL-RAW-Fc or control treatment **(F)**. All the immune cells were gated on parent immune cell CD45+ population. Data represent mean ± SEM. Student's t-test was used to calculate the significance of the difference between the groups. *p<0.05, **p=0.001–0.01, ***p=0.0001–0.001.
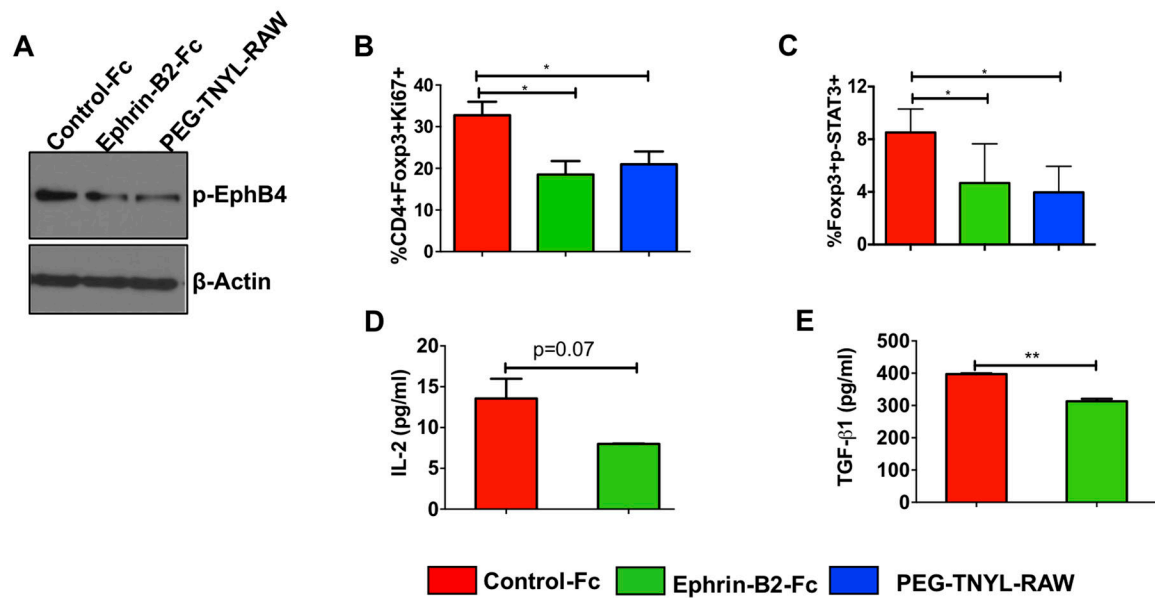
Figure 3. Treatment with a high (inhibitory) concentration of ephrin-B2-Fc reduces Ki67-expressing Tregs, STAT3 phosphorylation, and TGF-β1 and IL-2 levels in Tregs *in vitro*.
Western blot analysis of isolated CD4+ T cells treated with 20 μg/ml ephrin-B2-Fc for 72 hours shows a decrease in EphB4 tyrosine phosphorylation as compared to the control treatment group (2.5 μg/ml). PEGylated TNYL-RAW (EphB4 antagonist) show similar effect **(A)**. Flow cytometry analysis of T cells demonstrates decreased Ki67-expressing Tregs (CD4+Foxp3+Ki67+) following a 48 hour treatment with a high dose (20 μg/ml) of ephrin-B2-Fc or PEG-TNYL-RAW (4.5 μg/ml) **(B)**. The concentration of 20 μg/ml ephrin-B2-Fc has an inhibitory effect on p-STAT3 at the 24 hours time-point, similar to 4.5 μg/ml PEG-TNYL-RAW **(C)**. Conditioned media collected at 24 hours from Tregs treated with control-Fc, and 20 μg/ml ephrin-B2-Fc were subjected to TGF-β1 ELISA assay or to a U-plex mesoscale cytokine array to determine change in secreted IL-2 levels **(D)** and TGF-β1 levels **(E)**. Data represent mean ± SEM. The Student's t-test or one-way ANOVA were used to calculate the significance of differences between the groups.*p<0.05, **p=0.001–0.01.

Figure 4. Inhibition of EphB4-ephrin-B2 interaction combined with RT induces significant tumor growth suppression in orthotopic model of HNSCC.

The experimental design is shown in **(A)**. Inhibition of EphB4-ephrin-B2 interaction through hydrodynamic injection of the TNYL-RAW-Fc plasmid (20 μg/2 ml PBS/mouse) enhances the sensitivity of Ly2 tumors to RT (10 Gy) **(B)**. The dot plot shows tumor volumes on day 20 post-tumor implantation and shows significant differences between control and experimental groups **(C)**. Tumor volumes of individual mice within a group are represented by spaghetti plots **(D)**. One-way ANOVA was used to calculate the significance of the differences between groups in figure C. Data represent mean ± SEM. *p<0.05, **p=0.001–0.01, ***p=0.0001–0.001.
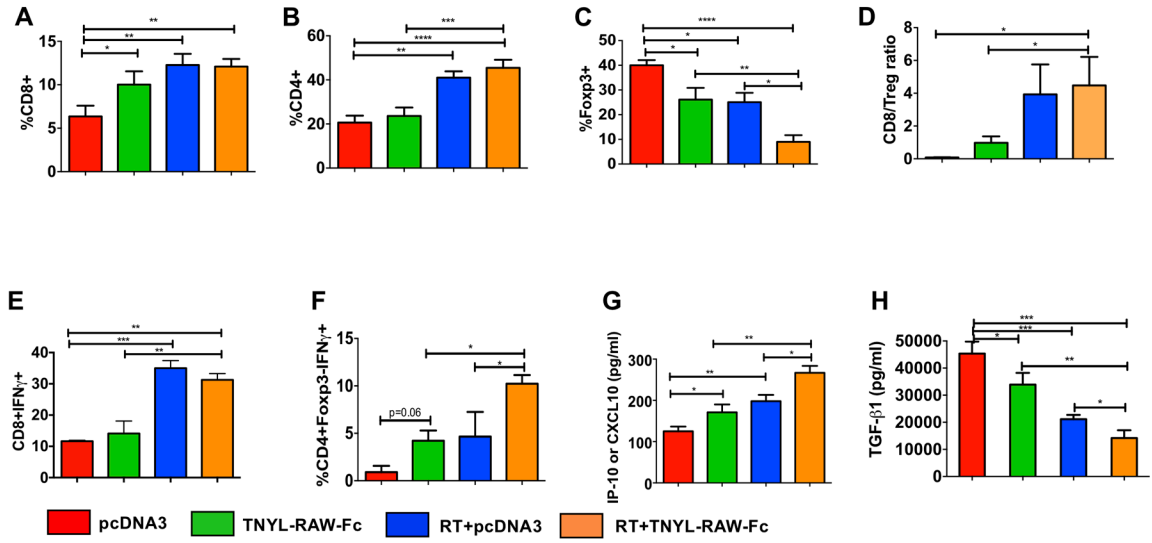
Figure 5. Inhibition of EphB4-ephrin-B2 signaling combined with RT inhibits HNSCC tumor growth by reducing Treg infiltrates and by enhancing activation of both CD4+Foxp3-conventional CD4+Foxp3- T cells and CD8+ T cells.

Tumors from control and experimental groups were harvested at 3 days after RT (10 Gy), processed and subjected to flow cytometry analysis. Data represent changes in immune infiltrates including CD8+ **(A)** CD4+ **(B)** Foxp3+ **(C)** cells and the CD8+ T cell/Treg ratio **(D)**. Flow cytometry analysis also shows an increase in the percentage of activated CD8+IFNγ+ **(E)** and CD4+Foxp3-IFNγ+ conventional CD4+Foxp3- T cells **(F)** in the combination group compared to the control and TNYL-RAW-Fc groups. Plasma samples were collected 3 days after RT and subjected to a U-plex mesoscale cytokine array or ELISA assay. An increase in the circulating IP-10/CXCL10 levels **(G)** along with a reduction in TGF-β1 **(H)** is evident in the combination treatment group compared to the control and single agent cohorts. One-way ANOVA was used to calculate the significance of the differences between the groups. Data represent mean ± SEM. *$p < 0.05$, **$p = 0.001$–0.01, ***$p = 0.0001$–0.001, ****$p < 0.0001$.
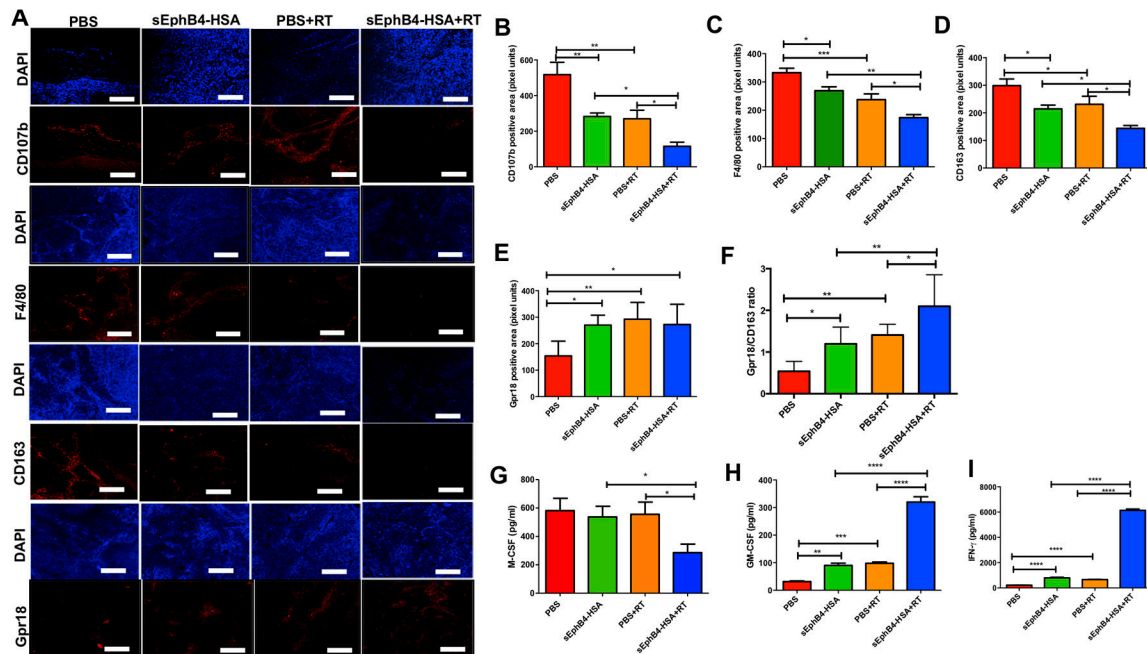
Figure 6. Targeting of EphB4-ephrin-B2 interaction combined with radiation decreases tumor-associated M2 macrophages in PDX models of HNSCC.
Immunofluorescence analysis shows decreased CD107b, F4/80, CD163, and increased Gpr18 staining in CUHN013 tumors treated with sEphB4-HSA and RT compared to single agents or the PBS control group **(A)**. CD107b and F4/80 represent pan-macrophage markers, CD163 is a specific marker for M2 macrophages and Gpr18 is a marker for M1 macrophages. Quantitative analysis for different macrophage markers is shown in **(B-F)**. Significant changes in the levels of inflammatory cytokines and chemokines are evident in plasma samples *in vivo* when EphB4-ephrin-B2 inhibition is combined with RT. Plasma samples were collected 96 hours after RT from the mice implanted with CUHN013 tumors and treated with PBS, sEphB4-HSA, PBS and RT, or sEphB4-HSA and RT and analyzed using a mouse cytokine array **(G-I)**. One-way ANOVA was used to calculate the significance of the differences between the groups. Data represent mean ± SEM. *$p<0.05$, **$p=0.001$–0.01, ***$p=0.0001$–0.001, ****$p<0.0001$. Scale bar: 100 μm.